

Vision-Language Modeling with Regularized Spatial Transformer Networks for All Weather Crosswind Landing of Aircraft

Debabrata Pal¹, Anvita Singh², Saumya Saumya¹, Shouvik Das¹

Aerospace, Honeywell Technology Solutions

¹Bengaluru, Karnataka 560103, India, ²Hyderabad, Telangana 500032, India
{Debabrata.Pal, Anvita.Singh, Saumya.Saumya, Shouvik.Das}@honeywell.com

Abstract—The intrinsic capability to perceive depth of field and extract salient information by the Human Vision System (HVS) stimulates a pilot to perform manual landing over an autoland approach. However, harsh weather creates visibility hindrances, and a pilot must have a clear view of runway elements before the minimum decision altitude. To help a pilot in manual landing, a vision-based system tailored to localize runway elements likewise gets affected, especially during crosswind due to the projective distortion of aircraft camera images. To combat this, we propose to integrate a prompt-based climatic diffusion network with a weather distillation model using a novel diffusion-distillation loss. Precisely, the diffusion model synthesizes climatic-conditioned landing images, and the weather distillation model learns inverse mapping by clearing those visual degradations. Then, to tackle the crosswind landing scenario, a novel *Regularized Spatial Transformer Networks* (RUSTAN) learns to accurately calibrate for projective distortion using self-supervised learning, which minimizes localization error by the downstream runway object detector. Finally, we have simulated a clear-day landing scenario at the busiest airport globally to curate an image-based Aircraft Landing Dataset (AIRLAD) and experimentally validated our contributions using this dataset to benchmark the performance.

Index Terms—visual landing, stable diffusion, spatial transformer networks, runway detection, aircraft landing dataset

I. INTRODUCTION

Vision-based aircraft landing or visual landing utilizes visual cues from aircraft camera data to assist a pilot during the landing phase. This approach acts as a reliable alternative to Instrument Landing Systems (ILS) and is essential for emergency landing at unprepared airfields with no ground-based navigation system. By providing real-time images of the runway and its surroundings, visual landing helps pilots gain enhanced situational awareness, especially while landing on short, unknown runways and in low visibility conditions such as fog, rain, or snow. Owing to the tremendous importance of visual landing, modern-day aircraft like Airbus A380 and Boeing 747 are being equipped with external cameras [1].

In extremely harsh weather, visibility degrades radically, challenging the usage of visible spectrum as landing assistance. To combat, the standard industrial solutions are Enhanced Vision System (EVS) and Synthetic Vision System (SVS) [2]. Even though using the infrared spectrum, EVS

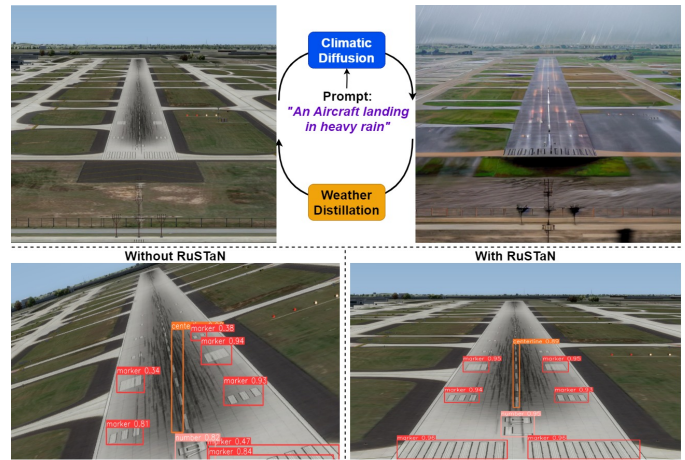


Fig. 1. a) Using prompt-based climatic diffusion, we generate landing images with harsh weather, and then the weather distillation module learns to clear visual degradations. During real-time inference, the trained weather distillation module generates clear weather landing images before detecting runway objects. b) The proposed RUSTAN module predicts accurate affine parameters to warp an image with a vertical axis parallel to the runway. It helps the predicted bounding boxes to converge to true runway object locations.

provides weather impact-free clean images, but the lack of color information causes pilot disorientation. On the other hand, SVS leverages a pre-stored terrain database to display positional information but misses real-time traffic data. It motivates us to utilize pilot-friendly visible spectrum only for landing assistance but pay special attention in removing the visual degradation artifacts due to the harsh weather scenarios.

Recently, leveraging the deep-learning-based Generative Adversarial Networks (GAN) [3], Weather GAN [4] and other weather translation models [5] have attempted to transfer the weather conditions of an image from one class to another, such as sunny-to-rainy, sunny-to-snowy, etc. Essentially, they exploited the deep semantic relationship of familiar weather cues, like blue sky, cloud, wet ground, and more. Nevertheless, a few potential drawbacks exist in directly adapting these weather translation models to the aviation industry to remove harsh weather visual artifacts. First, obtaining aerial data is quite costly. Then, the distance between a runway and the point where an aircraft prepares for descending is significantly high

and it allows weather to play a dominant role in obscuring the visibility. Also, unlike automobile industries, it is impossible to repeatedly fly an aircraft through the same geographical coordinates to obtain a pixel-paired real dataset. i.e., capturing the same runway images from the same viewing angle, velocity, altitude, latitude, and longitude during rain, fog, sunlight, etc. Besides, aerial photos suffer from projective distortions due to wind velocity, flight control, crosswind landing, etc.

Instead of obtaining real aerial data, acquiring equivalent simulation data (i.e. Unreal Engine [6]) for landing at a specific airport involves configuring multiple weather parameters. Repeating the same experiment for numerous airports globally is a huge labor-intensive task. As an alternative, CycleGAN [7] allows the translation of visual artifacts across diverse weather conditions by learning from unpaired data but requires a large-scale landing dataset under different weather categories. This is often impractical in our aerial data acquisition context and lags granular finetuning to capture visual landing scenarios with a mixture of different weather conditions. This motivates our first research question: “*Can we generate different weather-conditioned images from simple textual prompts?*” Effectively, it relaxes the need to acquire large-scale real landing images under diverse climatic variations.

The recent emergence of Vision Language Models (VLM) based on stable diffusion [8] can generate photo-realistic images from textual prompts. Further, ControlNet [9] allows the image generation to be controlled by additional depth maps, edge or pose images. Once the prompt-based diffusion model generates different weather-conditioned images, we can obtain a clean and harsh weather-paired dataset of the same landing scene. Then, a disjoint model can learn to distill weather artifacts from harsh weather counterparts (Fig. 1a). However, this disentangled diffusion of weather artifacts and filtering by a separate distillation model causes the poor generation of clear weather landing images. The optimization could be optimal if the distillation model can learn from the weather diffusion model to make the inverse mapping easier. It triggers second research question, “*Can we constrain an optimization objective to ensure that the weather distillation model learns an inverse relation with harsh weather diffusion network?*”

An on-ground trained object detector can be deployed inside an aircraft to recognize runway elements and aid in visual landing. However, due to crosswind landing and flight control, an aircraft can fly in real-time with angular deviation where the vertical axis of aircraft camera image is no longer parallel to a runway. It requires a large runway annotated dataset with different aircraft rolling, pitching parameters, and shifts from the runway for training a reliable runway object detector. However, data annotation is quite costly as it involves domain experts. It motivates us “*Can we learn from limited annotated runway dataset and perform a real-time projective transformation so that the warped image’s vertical axis becomes parallel to the runway?*”. In effect, it minimizes deviation from the actual location of runway elements (Fig. 1b). Finally, we observe that the “*unavailability of a benchmark aircraft landing image dataset impedes research on visual landing.*”

Our contributions: We propose a diffusion-distillation loss to guide the weather distillation model in learning the inverse relationship with the climatic diffusion model. Then, to learn landing at crosswind, we introduce a Regularized Spatial Transformer Networks (RUSTAN), which directly optimizes existing STN’s [10] Localization Net with randomly sampled known affine parameters. During inference, (RUSTAN) acts as a regular STN but performs superior in predicting the optimal affine parameters so that the warped camera image’s vertical axis becomes parallel to the runway. Finally, we introduce a simulation image-based Aircraft Landing Dataset (AIRLAD) with a clear-day landing scenario at the busiest airport, Hartsfield-Jackson Atlanta International Airport, to elevate the research on visual landing. Instead of simulating different weather conditions, our notion is to leverage VLM in composing complex weather mixtures by simple prompts and reduce paired dataset formation time. To summarize,

- Formulated diffusion-distillation loss to optimize climatic diffusion network and weather distillation model jointly.
- Proposed RUSTAN to precisely warp real-time camera data at crosswind landing, making reliable runway object detection.
- We curated a clear-day aircraft landing image dataset.

II. RELATED WORK

The traditional computer-vision-based runway detection employs HOG descriptors [11] due to photometric invariance but fails to deal with orientation. Damian *et al.* [12] apply a series of segmentation, contour, and line filtering steps with several rules per frame to measure relative aircraft position to the runway, but its computational complexity impedes real-time deployment. To generalize, an Airport Runway Detection Network (ARDN) [13] employs a region-based convolutional neural network (R-CNN) but can not deal with harsh weather impacts. LaneNet [14] and PointLaneNet [15] detect lane markings for automobiles but can not be adapted to the aviation industry due to huge weather impacts at a prolonged distance from the runway. Applying YOLOv5 to detect objects on the runway [16] does not validate its performance during the approach phase and crosswind landing. Overall, no runway detection research exists under dynamic weather conditions with versatile projective distortions during the approach stage.

III. PROPOSED METHOD

A. Problem Statement

We address the problem of recognizing essential runway elements under harsh weather conditions for monocular vision-based safe aircraft docking. Landing in extreme weather impacts clear visibility. Also, a non-linear projective transformation distorts the onboard camera data, especially while docking at a heavy crosswind, which must be calibrated first for the reliable localization of the runway elements. In *section B*, we analyze the contemporary approach and find its drawbacks in restoring projective distortion. Then, the newly proposed regularization technique is elaborated in *section C*. Finally, we describe the end-to-end vision-based aircraft landing pipeline (Fig. 3) with a novel climatic synthesis method in *section D*.

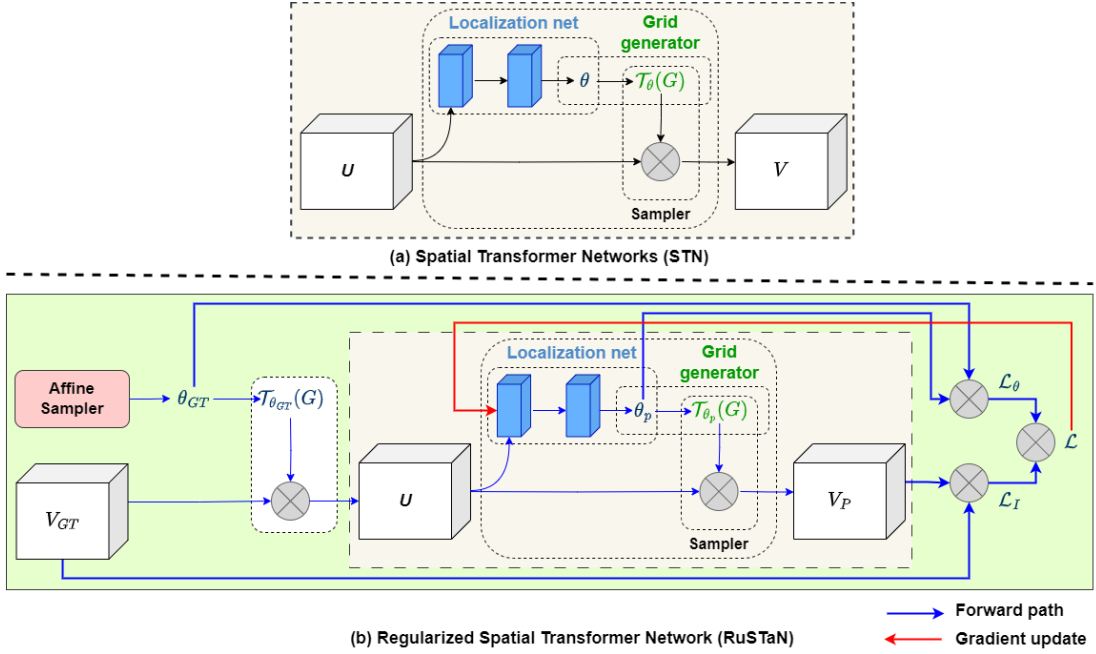


Fig. 2. a) In STN, a Localization Net predicts the transformation parameter θ , and an input image or a feature map is warped based on $\mathcal{T}_\theta(G)$. Due to the vanishing or exploding gradient problem in deep networks, θ can be inaccurate. Hence, in b), we regularize Localization Net to predict transformation parameter θ_p as θ_{GT}^{-1} during training, where θ_{GT} is obtained by a novel affine sampler. During inference, RUSTAN acts as STN where Localization Net directly processes the real-time projective distorted landing image U to predict accurate θ based on its self-supervised pre-training with inversion constraint.

B. Review of the Spatial Transformer Networks:

STN [10] consists of a Localization Net, a grid generator and is followed by a sampler, as shown in Fig. 2a. Incorporating STN in a CNN model, we gain spatial invariance to different geometric variations such as translation, rotation, scaling, and non-rigid skew deformation, etc. Basically, an STN module in a CNN classifier transforms an input image to a canonical shape and adapts its parameters by backpropagation from the final classification layer. The Localization Net predicts the optimal affine parameters, and the grid generator with a sampler performs bilinear transformation. For a 2D affine transformation, the affine matrix (\mathcal{A}_θ) can be defined,

$$\begin{pmatrix} x_i^s \\ y_i^s \end{pmatrix} = \mathcal{T}_\theta(G) = \mathcal{A}_\theta \begin{pmatrix} x_i^t \\ y_i^t \end{pmatrix} = \begin{bmatrix} \theta_{11} & \theta_{12} & \theta_{13} \\ \theta_{21} & \theta_{22} & \theta_{23} \end{bmatrix} \begin{pmatrix} x_i^t \\ y_i^t \end{pmatrix} \quad (1)$$

Where, an input image U is warped by an affine transformed regular grid G , $\mathcal{T}_\theta(G)$, to produce an output image V . (x_i^s, y_i^s) and (x_i^t, y_i^t) are the normalized regular grid G coordinates of U and V with spatial bounds as $[-1, 1]$.

However, we observe that STN suffers from a few major drawbacks: a) a model with deeper layers suffer from the vanishing or exploding gradients, which impacts the Localization Net of STN, causing inaccurate affine or projective transformation parameter prediction, b) different objects with varied geometric transformations in a scene can reduce prediction confidence of Localization Net. In effect, the incorrect geometric warping by the STN sampler impacts the downstream applications such as object detection, tracking, etc.

C. Novel Regularized Spatial Transformer Networks:

To combat the aforementioned challenges of STN, we perform a self-supervised training [20] of the Localization Net.

Our proposed approach is inspired by deep supervision [17], allowing better gradient flow in a classification network. First, we introduce an Affine sampler that produces known affine parameters, θ_{GT} for the arbitrarily selected translation (t_x, t_y) , rotation (ϕ) , scaling (S_x, S_y) values,

$$\theta_{GT} = \begin{bmatrix} 1 & 0 & t_x \\ 0 & 1 & t_y \\ 0 & 0 & 1 \end{bmatrix} \begin{bmatrix} \cos \phi & -\sin \phi & 0 \\ \sin \phi & \cos \phi & 0 \\ 0 & 0 & 1 \end{bmatrix} \begin{bmatrix} S_x & 0 & 0 \\ 0 & S_y & 0 \\ 0 & 0 & 1 \end{bmatrix} \quad (2)$$

Then, we obtain a sampling grid by warping a regular grid with $\mathcal{T}_{\theta_{GT}}(G)$. An input image or feature map V_{GT} is then bilinear transformed by the new sampling grid, producing deformed U . The Localization Net in STN predicts affine parameters, θ_p . Further transforming deformed U with $\mathcal{T}_{\theta_p}(G)$, we obtain V_p . Ideally, the reverse warped V_p should be equal to V_{GT} . Thereby we regularize the Localization Net to predict θ_p as θ_{GT}^{-1} . The RUSTAN module is shown in Fig. 2b and is constrained with two optimization objectives during training,

$$\begin{aligned} \mathcal{L}_\theta &= \frac{1}{N} \sum_{i=1}^N (\theta_{GT} - \theta_p)^2; \mathcal{L}_I = \|V_{GT} - V_p\|_1; \\ \mathcal{L}_{\text{RUSTAN}} &= \lambda_1 * \mathcal{L}_\theta + \lambda_2 * \mathcal{L}_I \end{aligned} \quad (3)$$

Where, \mathcal{L}_θ and \mathcal{L}_I are the loss components for optimizing affine parameters and images, respectively. λ 's are the coefficients for the loss components. $N = |\theta_{GT}| = |\theta_p|$, where $|\cdot|$ denotes the cardinality operator. In this experiment, we consider \mathcal{L}_θ as mean squared error loss and \mathcal{L}_I as mean absolute error loss. During inference, the projective distorted images U are directly processed by pre-trained Localization Net of RUSTAN and are expected to produce accurate canonical output, which helps in further downstream applications.

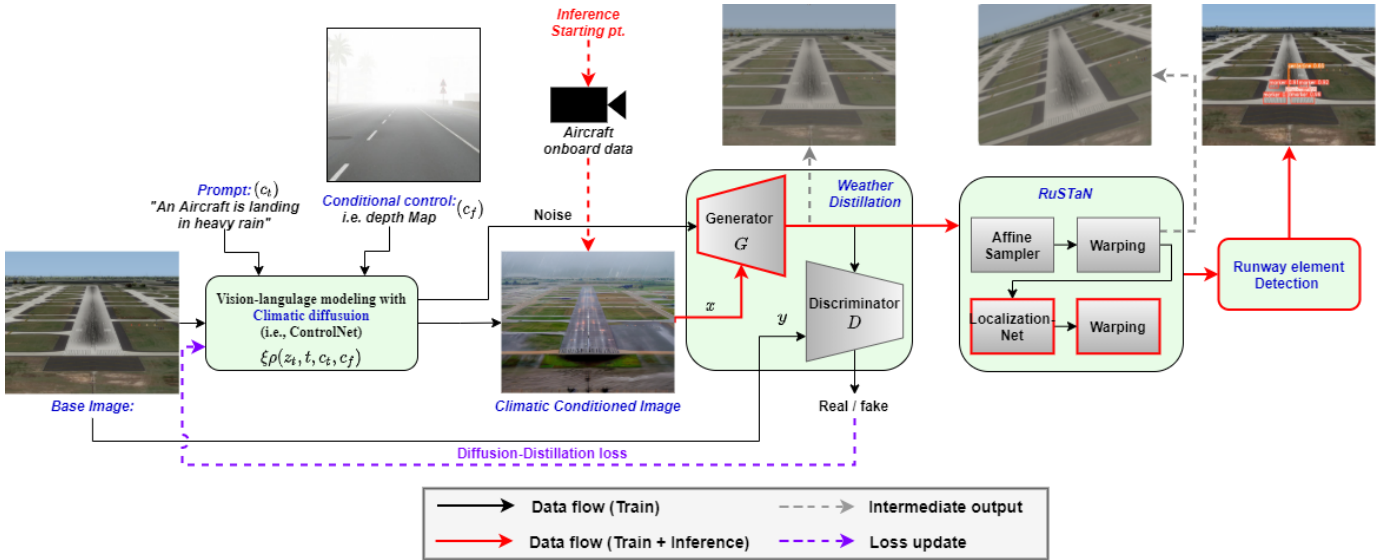


Fig. 3. Illustration of the proposed framework. During training, diverse harsh climatic conditions are synthesized using a VLM, and a generative weather distillation module learns to remove the synthesized weather artifacts. Besides, to learn to recognize runway elements during landing at crosswind, the affine sampler in the RUSTAN module geometrically distorts an input image and, followed by a Localization Net, learns to restore from the projective transformation. Finally, an object detector localizes essential runway elements to aid the pilot in a vision-based landing. Inference time data flow is highlighted in ‘Red’ color, which relaxes VLM and affine sampler usage as weather degradation and projective distortion at crosswind can inherently impact the real-time camera data.

D. Proposed framework

The proposed architecture is shown in Fig. 3, and below, we summarize the individual modules of our architecture.

i) *Proposed prompt-driven self-supervised learning*: Our dataset contains aircraft landing images in clear day scenarios. However, in real life, a pilot faces extreme weather, reducing the visibility. To simulate the impact of degraded weather and learn to nullify the visual deterioration, we introduce climatic diffusion and weather distillation modules, respectively.

- *Climatic diffusion*: We leverage a text-to-image diffusion model, ControlNet [18], for spatial conditioning of climatic condition. Precisely, we control the weather artifacts, i.e., smoke, fog, etc., through a depth map as the severe weather artifacts in images get increased with distance from the aircraft. Besides, we fine-tune ControlNet with customized templates. For example, “An aircraft is landing in heavy {*weather_condition*}”, where the variable *weather_condition* can have values as {“rain”, “fog”, “smoke”, “haze”}, etc.
- *Weather distillation*: Once we obtain a paired correspondence of the degraded weather and a clean landing image, we learn to minimize pixel reconstruction loss. For this purpose, we use Pix2Pix [19], a Generative Adversarial Network (GAN)-based image-to-image translation framework. During real-time landing, the pre-trained Pix2Pix distills weather artifacts to generate clear landing images.
- *Novel diffusion-distillation loss*: During training, we stitch the disentangled generation of harsh weather with its distillation counterpart in the self-supervised learning [20] approach. The training objective becomes,

$$\mathcal{L} = \mathbb{E}_{y, z_0, t, c_t, c_f, \epsilon \sim \mathcal{N}(0,1)} \|y - G(x, \xi\rho(z_t, t, c_t, c_f))\|_1; \quad (4)$$

Where, y is the target clear day image, and $\xi\rho$ is the frozen diffusion network of ControlNet with intermediate noisy image z_t sampled from Gaussian noise $\epsilon \sim \mathcal{N}(0,1)$. At each time step t of climatic diffusion, $\xi\rho$ predicts the amount of noise added to z_t given a textual prompt c_t , and a conditional control (i.e., depth map) c_f . Leveraging this predicted noise and ControlNet-generated harsh weather image x , the Pix2Pix generator G synthesizes clear-day images. The L1 loss (Manhattan distance) between y and G output is used to optimize Pix2Pix GAN components at each time step. Even though without $\xi\rho$ prediction, G could map x to y , the inclusion of it enables diversity to rectify from various distributions of climatic conditions.

ii) *Geometric distortion calibration by RUSTAN*: The Pix2Pix generator (G) outputs an aircraft landing image free from atmospheric effects, which is then calibrated by the RUSTAN module to obtain canonical representation. The projective transformation warps the input video frame to align the runway parallel to the vertical axis of the image plane. It helps the downstream object detector for reliable localization of the runway elements due to getting pre-trained with ground-truth annotations at no tilting angle of an aircraft.

iii) *Runway object detection*: Using YOLO v8 [21], we detect different runway elements, i.e., runway centerline, markers, numbers, etc. It helps the pilot perform a vision-based dock at the designated runway number despite having degraded visibility and glide over the runway center, thus minimizing any probable wingtip collisions with surrounding airport objects.

iv) *Inference steps*: First, the aircraft camera data passes through G of the weather distillation module to eliminate any harsh weather impact. Then, it is geometrically calibrated by Localization Net predicted parameters due to landing at varied attitudes. Finally, different runway elements are recognized.

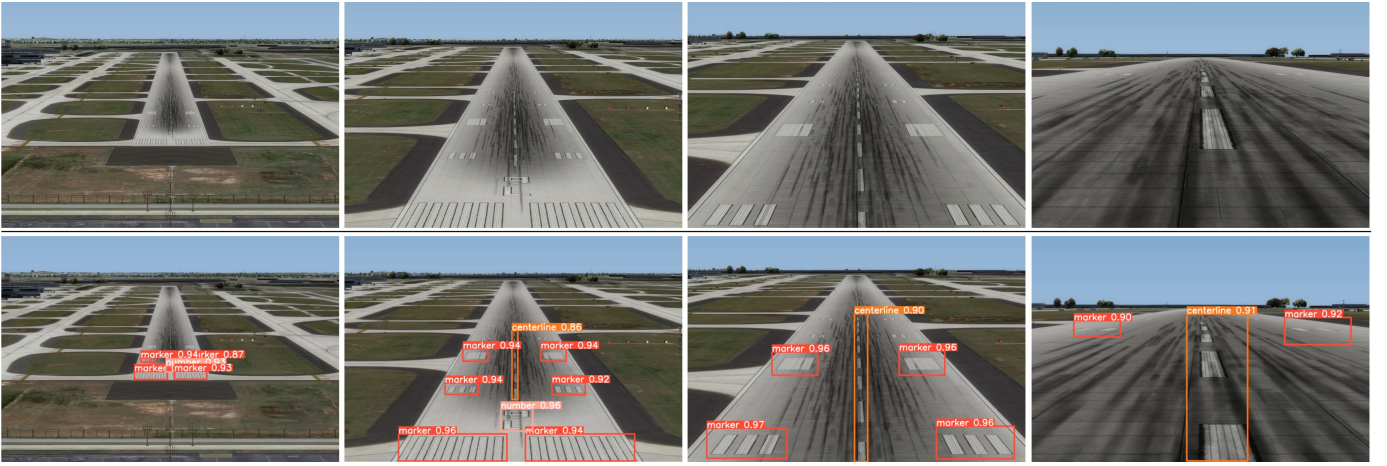


Fig. 4. (Row 1) Sample images of the AIRLAD dataset featuring aircraft landing at KATL airport. (Row 2) Bounding boxes of the detected runway elements by YOLO v8 with corresponding confidence scores are annotated. Thanks to RUSTAN module for effectively projecting images at a vertical axis parallel to the runway even though input images are rotated at 5° to mimic the crosswind landing scenario. Overall, it reduces the high divergence or localization error of the predicted bounding boxes from the actual canonical representation and minimizes the overlap between bounding boxes of nearby runway elements.

TABLE I
COMPARATIVE ANALYSIS OF THE RUNWAY OBJECT DETECTION PERFORMANCE WITH AND WITHOUT RUSTAN

Angular deviation	W/o STN / RuSTAN				With STN				With RuSTAN			
	P	R	mAP50	mAP50-95	P	R	mAP50	mAP50-95	P	R	mAP50	mAP50-95
0°	0.99	0.97	0.99	0.90	0.99	0.95	0.98	0.92	0.99	0.98	0.99	0.94
3°	0.88	0.90	0.91	0.40	0.91	0.92	0.93	0.71	0.95	0.95	0.96	0.82
5°	0.70	0.68	0.67	0.21	0.78	0.75	0.80	0.65	0.87	0.84	0.88	0.76
10°	0.13	0.12	0.10	0.03	0.55	0.58	0.56	0.47	0.75	0.72	0.79	0.61
15°	0.08	0.10	0.06	0.02	0.35	0.33	0.37	0.24	0.41	0.38	0.46	0.32

IV. EXPERIMENTS AND ANALYSIS

A. Dataset overview

The vision-based landing system plays a pivotal role in providing important visual cues during the critical phases of aircraft landing. Among thousands of airports globally, Hartsfield-Jackson Atlanta International Airport (ICAO: KATL) in the United States consistently secures the busiest airport ranking. ILS or any other subsystem failure in an aircraft significantly impedes landing, thus becoming a bottleneck for traffic management. It motivates us to develop a visual landing scenario for KATL airport, and we term this dataset AIRLAD (AIRport LAnding Dataset). We use a virtual aircraft model, Carenado Commander 114, to simulate the landing scenario using the Prepar3D flight simulation platform. The initial position is three nautical miles from the aiming point with an attitude of 3 degrees. The data is captured on a clear day at 11.00 AM GMT. Overall, the data contains 6,340 video frames at 30 FPS. The data is free from harsh climatic conditions to elevate the mixture with plausible weather distributions and create complex landing scenarios using Generative models. AIRLAD complements a few available runway detection datasets (i.e., LARD [22]) but explicitly focuses on landing at the busiest airport, KATL. Sample AIRLAD images are shown in Fig. 4 (Row 1).

B. Evaluation metrics

To evaluate the runway object detection performance, we use standard metrics, namely, Precision (P), Recall (R), F1

score, and Mean Average Precision (mAP). Precision quantifies the proportion of true positives among all positive predictions, assessing the model's capability to avoid false positives. On the other hand, recall calculates the proportion of true positives among all actual positives, measuring the model's ability to detect all class instances. The F1 score is the harmonic mean of precision and recall, providing a balanced assessment of a model's performance while considering both false positives and false negatives. mAP is computed by applying a threshold on Intersection over Union (IoU), which measures the overlap between predicted and ground truth bounding boxes, assessing the object localization precision. mAP50 represents mAP at the IoU threshold 0.50, evaluating model accuracy for easy detection. Whereas mAP50-95 averages mAP score across IoU thresholds of 0.50 to 0.95, providing a holistic view of model performance across various levels of detection difficulty [23].

$$\text{mAP50} = \frac{1}{N} \sum_{i=1}^N \text{AP}_i^{0.5} \quad (5)$$

$$\text{mAP50-95} = \frac{1}{N} \sum_{i=1}^N \text{AP}_i^{0.5-0.95} \quad (6)$$

Where, $\text{AP}_i^{0.5}$ represents the average precision for class i at IoU threshold 0.5 and $\text{AP}_i^{0.5-0.95}$ indicates the same for threshold ranging from 0.5 to 0.95. N is the number of classes, which is 3 in our case as we estimate detection performance for three runway classes: marker, centerline, and number.

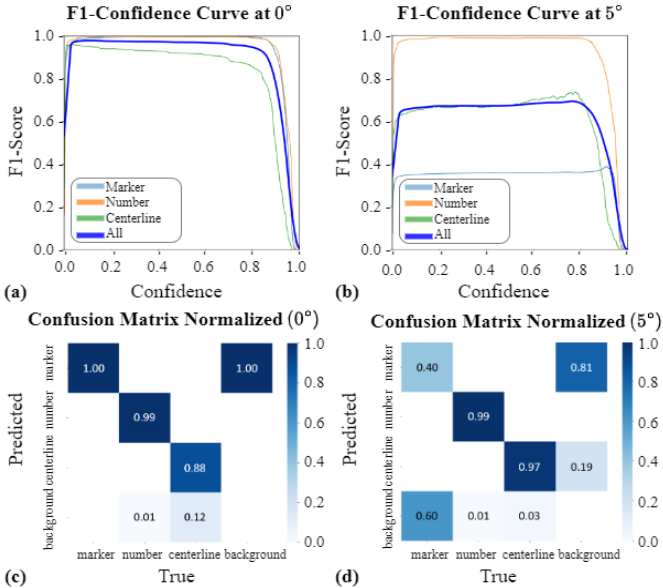


Fig. 5. The class-wise F1 scores in detecting runway objects from the 0° and 5° rotated test frames are shown in (a) and (b), respectively, to evaluate the crosswind landing performance without using STN or RUSTAN. Corresponding confusion matrices are shown in (c) and (d). Without spatial transformation, the localization error of the object detector steadily increases.

C. Experimental results

We train the proposed architecture in Fig. 3 for 500 epochs with Adam optimizer of learning rate $1e-5$ for three cases: a) without spatial transformation by STN or RUSTAN, b) with STN, and c) with RUSTAN and record the test performance in Table I. The test frames are rotated from 0° to 15° to evaluate the runway object detection performance at crosswind landing.

Without any spatial transformation, increasing angular variation of test data causes a sharp decline in object detection performance, especially at 15° rotation, where none of the runway objects are detected. Incorporating STN, the detection performance improved significantly due to the warping of rotated test images by the Localization Net predicted affine parameters before runway object detection. Effectively, this performance indicates the geometric transformation invariance nature by the learnable Localization Net. Further, utilizing the proposed RUSTAN, the detection performance drastically outperformed STN, particularly for deviations other than 0° . RUSTAN can quickly calibrate from arbitrary geometric distortions due to leveraging the Localization Net, which is trained by the proposed self-supervised learning approach.

The curves in Fig. 5 (row 1) illustrate how the F1-score changes as the confidence threshold varies for different angular variations of test images without any spatial transformation. At 0° , all the classes have a high F1-score, but it drops at 5° , specifically for the runway marker class having a high aspect ratio in image space. The second row of Fig. 5 indicates a comprehensive evaluation of the model’s confusion matrix under the same test scenario. At 0° , predicted false positives or negatives are minimal. Rotating test data to 5° raises the number of false positives, especially for the marker class.

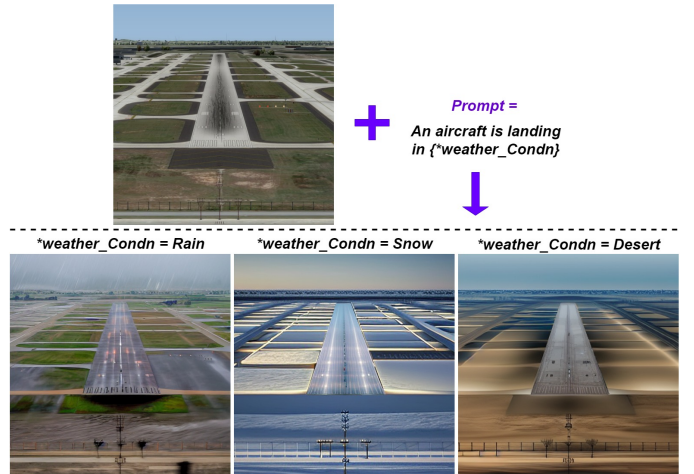


Fig. 6. The aircraft landing images generated by the climatic diffusion model using different prompt-driven climatic conditions, i.e., rain, snow, etc.

TABLE II
IMPACT OF OPTIMIZING WEATHER DISTILLATION MODEL WITH DIFFUSION-DISTILLATION LOSS

Diffusion-distillation loss	With RuSTAN, (5° rotation)			
	P	R	mAP50	mAP50-95
Without	0.81	0.83	0.79	0.68
With	0.87	0.84	0.88	0.76

D. Ablation analysis

i. Climatic-conditioned image generation: Using ControlNet [18], the climatic diffusion model generates landing images with visual degradations for different weather conditions. The generated images for a given clear-day landing image and a set of climatic-conditioned prompts are shown in Fig. 6. We consider depth map for spatial conditioning. Also, we record the seed value of the noise distribution to apply over other images in the dataset and maintain perceptual consistency while learning to land at an exact weather condition.

ii. Optimization with diffusion-distillation loss: The weather distillation module learns to restore clear-day images from the induced visual degradations by the climatic diffusion model. Optimizing the weather distillation module with the proposed diffusion-distillation loss helps to learn the inverse relationship in the latent space. Thus, we obtain clearer day images, allowing better runway object detection. In Table II, we evaluate the impact of this loss optimization considering the test frames have rotated by 5° for crosswind landing, and they are projective transformed by RUSTAN before object detection. Optimization with diffusion-distillation loss causes approximately 8% improvement of mAP50-95 metric.

iii. Runway object detection at crosswind landing: The Localization Net of STN predicts affine parameters, used to warp an image and restore from projective distortion. Further, we can obtain precise restoration of complex real-world images by performing self-supervised pre-training of Localization Net using RUSTAN. After being calibrated by RUSTAN from the 5° rotated test landing image, the detected runway objects are shown in Fig 4 (Row 2). Also, we perform a comparative

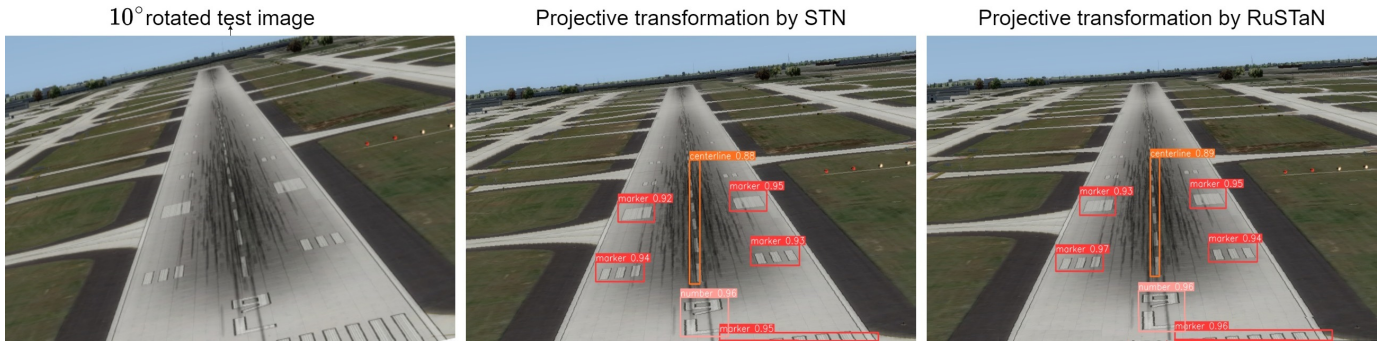


Fig. 7. Comparative analysis to restore from projective distortion after rotating test image by 10° .

study between STN and RUSTAN based on the warped images by the predicted affine parameters. We obtain a more precise runway parallel warped image by RUSTAN in Fig 7, resulting in better runway object detection with higher confidence.

V. CONCLUSION

This paper proposes a prompt-based visual weather degradation synthesis method to form a landing scenario paired dataset under clear-day and harsh weather conditions. Thereby, a novel diffusion-distillation loss helps optimize the weather distillation network to learn to remove the harsh weather visual artifacts. Further, directly optimizing the Localization Net of RUSTAN for the affine sampler predicted parameters causes to perform better runway object detection at crosswind landing. Experimental results over the proposed AIRLAD dataset and ablation analysis prove our real-time situational aware runway object detection capability for vision-based aircraft landing. In the future, we will apply optical character recognition to the detected runway number class images. Also, we plan to enlarge our dataset with real and simulation-based landing scenarios at other airports and evaluate the model performance.

REFERENCES

- [1] Meggitt "https://www.meggitt.com/products-services/aircraft-cameras/" (Last accessed: 01-30-2024).
- [2] Foyle, David C., Albert J. Ahumada, James Larimer, and Barbara Townsend Sweet. "Enhanced/synthetic vision systems: Human factors research and implications for future systems." *SAE Transactions* (1992): 1734-1741.
- [3] Radford, Alec, Luke Metz, and Soumith Chintala. "Unsupervised representation learning with deep convolutional generative adversarial networks." *arXiv preprint arXiv:1511.06434* (2015).
- [4] Li, Xuelong, Kai Kou, and Bin Zhao. "Weather GAN: Multi-domain weather translation using generative adversarial networks." *arXiv preprint arXiv:2103.05422* (2021).
- [5] Hwang, Sunhee, Seogkyu Jeon, Yu-Seung Ma, and Hyeran Byun. "WeatherGAN: Unsupervised multi-weather image-to-image translation via single content-preserving UResNet generator." *Multimedia Tools and Applications* 81, no. 28 (2022): 40269-40288.
- [6] Sanders, Andrew. *An introduction to Unreal engine 4*. CRC Press, 2016.
- [7] Zhu, Jun-Yan, Taesung Park, Phillip Isola, and Alexei A. Efros. "Unpaired image-to-image translation using cycle-consistent adversarial networks." In *Proceedings of the IEEE international conference on computer vision*, pp. 2223-2232. 2017.
- [8] Rombach, Robin, Andreas Blattmann, Dominik Lorenz, Patrick Esser, and Björn Ommer. "High-resolution image synthesis with latent diffusion models." In *Proceedings of the IEEE/CVF conference on computer vision and pattern recognition*, pp. 10684-10695. 2022.
- [9] Zhang, Lvmin, Anyi Rao, and Maneesh Agrawala. "Adding conditional control to text-to-image diffusion models." In *Proceedings of the IEEE/CVF International Conference on Computer Vision*, pp. 3836-3847. 2023.
- [10] Max Jaderberg, Karen Simonyan, Andrew Zisserman, et al., "Spatial transformer networks," *Advances in neural information processing systems*, vol. 28, 2015.
- [11] D. S. Andreev and N. V. Lysenko, "Objects Recognition Methods Estimation in Application to Runway Pictures Taken in Poor Visibility Conditions," 2019 IEEE Conference of Russian Young Researchers in Electrical and Electronic Engineering (EIconRus), Saint Petersburg and Moscow, Russia, 2019, pp. 1141-1145, doi: 10.1109/EIconRus.2019.8656649.
- [12] Kordos, Damian, Paweł Krzaczkowski, Paweł Rzucidło, Zbigniew Gomółka, Ewa Ześlawska, and Bogusław Twaróg. "Vision System Measuring the Position of an Aircraft in Relation to the Runway during Landing Approach." *Sensors* 23, no. 3 (2023): 1560.
- [13] R. A. Amit and C. K. Mohan, "A Robust Airport Runway Detection Network Based on R-CNN Using Remote Sensing Images," in *IEEE Aerospace and Electronic Systems Magazine*, vol. 36, no. 11, pp. 4-20, 1 Nov. 2021, doi: 10.1109/MAES.2021.3088477
- [14] Wang, Ze, Weiqiang Ren, and Qiang Qiu. "Lanenet: Real-time lane detection networks for autonomous driving." *arXiv preprint arXiv:1807.01726* (2018).
- [15] Chen, Zhenpeng, Qianfei Liu, and Chenfan Lian. "Pointlanenet: Efficient end-to-end cnns for accurate real-time lane detection." In *2019 IEEE intelligent vehicles symposium (IV)*, pp. 2563-2568. IEEE, 2019.
- [16] Muzalevskiy, Aleksandr R., Elena V. Serykh, Mihail M. Kopichev, and Evgenij V. Druian. "Runway Marking Detection using Neural Networks." In *2023 V International Conference on Control in Technical Systems (CTS)*, pp. 239-243. IEEE, 2023.
- [17] Chen-Yu Lee, Saining Xie, Patrick Gallagher, Zhengyou Zhang, and Zhuowen Tu, "Deeply-supervised nets," in *Artificial intelligence and statistics*. PMLR, 2015, pp. 562-570.
- [18] Zhang, Lvmin, Anyi Rao, and Maneesh Agrawala. "Adding conditional control to text-to-image diffusion models." In *Proceedings of the IEEE/CVF International Conference on Computer Vision*, pp. 3836-3847. 2023.
- [19] Isola, Phillip, Jun-Yan Zhu, Tinghui Zhou, and Alexei A. Efros. "Image-to-image translation with conditional adversarial networks." In *Proceedings of the IEEE conference on computer vision and pattern recognition*, pp. 1125-1134. 2017.
- [20] Misra, Ishan, and Laurens van der Maaten. "Self-supervised learning of pretext-invariant representations." In *Proceedings of the IEEE/CVF conference on computer vision and pattern recognition*, pp. 6707-6717. 2020.
- [21] Jacob Solawetz and Francesco. *What is yolov8? the ultimate guide.*, 2023. (Last accessed: 01-30-2024).
- [22] Ducoffe, M., Carrere, M., Féliers, L., Gauffriaux, A., Mussot, V., Pagetti, C., Sammour, T. (2023). LARD – Landing Approach Runway Detection – Dataset for Vision Based Landing. *ArXiv. /abs/2304.09938*.
- [23] Ultralytics YOLOv8 Docs "https://docs.ultralytics.com/guides/yolo-performance-metrics/" (Last accessed: 01-30-2024).